Thrombosis Journal

BioMed Central

Original basic research

Open Access

# MRI of coronary artery atherosclerosis in rabbits: Histopathology-MRI correlation and atheroma characterization

Rakesh Sharma*[1] and Ram B Singh[2]

Address: [1]Department of Medicine, Columbia University, New York, NY 10032 USA and [2]Heart Research Medical Center, Moradabad 14107, UP, India

Email: Rakesh Sharma* - rs2010@columbia.edu; Ram B Singh - icn@mickyonline.com

* Corresponding author

Published: 15 May 2004

*Thrombosis Journal* 2004, **2**:5

Received: 31 December 2003
Accepted: 15 May 2004

This article is available from: http://www.thrombosisjournal.com/content/2/1/5



## Abstract

**Background and objectives:** We report *in vivo* magnetic resonance imaging (MRI) characteristics and histopathology correlation of the thrombus formation in atherosclerosis the rabbit animal model.

**Design and methods:** Atherosclerosis was induced in white male rabbits with vegetable ghee followed oxidized diet. Baseline MRI of atherosclerosis-recruited rabbits was done and later animals were used for atheroma histopathology characterization. Contiguous cross-sectional T2-weighted fast spin echo MRI images were compared by coronary histopathology. In all animals, coronary aortic wall thickening and atheroma size was measured using MRI.

**Results:** MRI images and digitized histological sections confirmed intraluminal thrombus in 6 (67%) of the 9 animals. MRI data showed correlation with the histopathology for aortic wall thickness ($R^2$ = 0.82, P < 0.0001), lumen area ($R^2$ = 0.88, P < 0.0001) and plaque size ($R^2$ = 0.77, P < 0.0001). Optimized TE and TR parameters and multicontrast enhancement generated better MRI visibility of vulnerable plaque components. The MRI data evaluated % stenosis, plaque burden. Frequency of plaques, plaque height in aorta and coronary artery atheroma was also assessed by histology. In vivo, MRI determined the presence and size of the thrombus in this animal model of atherosclerosis and histopathology defined the plaque disruption.

**Conclusion:** The combination of in vivo MRI and comparison with histopathology images of rabbit coronary thrombus may be a research tool for understanding of the pathogenesis of acute coronary plaques.

## Introduction

Cardiovascular risk assessment was reported by the identification of flow-limiting coronary stenoses, wall thickness, and plaque burden and its components in rabbit experimental model [1] and risk dependence on lipid intake in diet [2]. The mechanism of acute coronary syndromes is understood due to the disruption of an atherosclerotic coronary plaque with an overlying thrombus [3a, 3b, 4]. Still coronary artery atheroma development and plaque constituents are not well documented. In vivo/ex vivo MR microimaging (MRM) is emerging as a noninvasive modality in assessment of cardiovascular risk but has

not been applied to acute coronary syndromes and plaque chemical composition [5]. Using a rabbit experimental model [1], we evaluated MRI visible plaque features and compared with morphometric histology features with object if MRM can detect a thrombus overlying an atherosclerotic plaque at optimized MRI scan parameters with enhanced multi-contrast.

## Materials and methods

### *Experimental rabbits and diet*

Nine adult male white rabbits weighing 500 gm were observed for 12 weeks after the animals reached at least 1.0 kg adult body weight gain and 12 months age. These animals were scheduled on 12-week diet period on a high trans fatty acid (TFA) rich diet (supplemented with aluminum hydroxide placebo and vegetable ghee 7.2 gm/day) to develop hyperlipidemia and atherosclerosis after which they were randomized to intervention and control groups. Rabbit chow was treated with ferric chloride (5 mg/day) complexed with EDTA in equal proportions to keep ferric iron in the solution to stimulate peroxidation in rabbits. A double dose of vitamin C (10 mg/day) was added to this chow to produce ferrous ion, which is powerful oxidant. After 16 weeks, rabbits were fed oxidized rabbit chow for 4 weeks as described elsewhere [1].

### *In vivo MRI study protocol*

Rabbits were anesthetized by using intramuscular ketamine (30 mg/kg), xylazine (5 mg/kg). The animals were placed prone in the MRI scanner table under respiratory gating. All scans were performed on a 1.5-T LX Horizon GE Signa MR scanner (GE Medical Systems) by use of an UltraImage cardiac phased-array coil for better signal noise ratio. MRI of normal rabbits was performed followed by 8-week high cholesterol diet and these animals underwent MRI examination. The coronary aortic localizer consisted of a fast multislice multistack (transverse) segmented Gradient Echo (GE) localizer scan of the thorax. Scan parameters were: TR = 10 ms, TE = 2.5 ms, flip angle 35°, slice thickness 1 mm, field of view 128 × 128 $mm^2$, and matrix 128 × 64. Transverse images of the coronary aorta (1 mm) were obtained along the major axis of the right coronary aorta (RCA), left anterior descending (LAD) and left circumflex (LCx) arteries. For transverse coronary wall imaging, fat-suppressed T2-weighted fast spin echo scans were acquired to assess cross-sectional views of aortic vessel. Scan parameters were: 24 contiguous slices, TE = 80 ms, TR ≃ 5 R-R intervals, slice thickness 3 mm, field of view 128 × 128 $mm^2$, and matrix 256 × 256, echo train length 10 and minimum spacing ~9 ms [6]. The total imaging time for the T2-weighted scan was 15–18 minutes at the heart rate 140 bpm.

### *Multislice Gradient Echo (GE) sequence*

The basic gradient-echo sequence has two distinct sections: slice selection and image encoding. Applying a magnetic field gradient perpendicular to the desired slice orientation performed slice selection. The applied gradient varied linearly along the gradient axis. This gradient induced a radiofrequency (RF) pulse, which generated resonance spread over a thin band of tissue to give off a magnetic resonance detectible signal. Images were acquired as 2D slices. For coronary artery imaging, the basic GE sequence was applied many times in rapid succession so that Gradient-echo last for 8 msec. During each application the amplitude of the phase encoding gradient was stepped to a new phase encoding value. Slices were acquired in contiguous manner while slices were selected in rapid succession. Motion was minimum between adjacent slices that provided reasonable continuity of coronary sections between slices.

### *Contrast enhancement and parametric MR microimaging at 9.4 T*

For contrast enhancement plots, only coronary plaques with > 2 $mm^3$ volume were obtained fresh in saline and later cold packed for immediate MR imaging (n = 8). For scan parameters optimization, 9.4 T multi-slice spin echo images were obtained on 'Varian 400 Utility' at 7 discrete echo times (TE = 20–80 ms) with repetition time (TR = 4 sec) and 8 transients per acquisition. TE and TR values were plotted in 3D. These images sets were analyzed by Optimas 6.5 software to produce a parametric T2 image for selected slices. With sample position maintained, an additional image data set was collected at TE = 30 ms and TR arrayed at 8 discrete delays (0.3–8 sec) for saturation recovery. This image set was also analyzed to yield a parametric T1 image for selected slices [5].

With a multicontrast protocol using T1-weighted, proton density-weighted and T2-weighted images, area of coronary tissue features were measured [5].

### *Tissue preparation for histopathology*

The coronary arteries from the rabbits were immediately excised after MR imaging and cut into 16 serial 2.5-mm segments matching corresponding MR images. Using landmark coronary branch performed coregistration. For histological examination, aorta were decalcified in 1% formalin, 4-micron sections were cut, mounted and processed for staining with hematoxylin-eosin and trichrome staining of neutral lipid, calcium, fibrous and cellular components. The morphology of aortic lesions and atheroma pathological changes were assessed using a Polaroid photo scanner at 335 dpi. Each single section was scanned for the numbers of atherosclerosis plaques in different coronary arteries (n = 16). Exact diameter of coronary artery on slide was measured by view-scale to create

**Table 1: In control group animals plaque morphology indices were negligible (shown as none) while atherosclerosis group animals showed different mean ± s.d. values for extent of atherosclerosis in rabbits (n = 9). Extent of atherosclerosis is shown as aortic sudanophilia score, aortic and coronary artery atherosclerosis scores (% scores) and plaque heights(in μm).**

| Plaque Morphology Index | Control Group | Atherosclerosis Group |
|---|---|---|
| Aortic sudanophilia (% score) | none | 17.5 ± 3.3 |
| Aortic plaque height (μm) | none | 345 ± 8.8 |
| Coronary plaque height (μm) | none | 87.6 ± 8.6 |
| Coronary atherosclerosis index | none | 16.6 ± 3.2 |
| Aortic atherosclerosis score | none | 14.3 ± 3.1 |
| Coronary atherosclerosis score | none | 5.60 ± 0.8 |

**Table 2: In control group animals, frequency of plaques, ulceration and thrombosis were negligible (shown as none) while atherosclerosis group animals showed different mean values for plaque frequency, ulceration and thrombosis in rabbits (n = 9). Frequency of plaques, ulceration and thrombosis are shown in atherosclerosis group of rabbits (n = 9).**

| Plaque Atheroma Index | Control Group | Atherosclerosis Group |
|---|---|---|
| Aortic plaque frequency | none | 51.3 |
| Coronary plaque frequency | none | 26.8 |
| Aortic plaque ulceration | none | 18.2 |
| Coronary plaque ulceration | none | 16.6 |
| Aortic plaque thrombosis | none | 12.6 |
| Coronary plaque thrombosis | none | 14.5 |
| Aortic plaque cracks/fissures | none | 17.2 |
| Coronary plaque cracks/ fissures | none | 1.64 |

**Table 3: The Table represents the area (in $mm^2$) and % MR signal intensity (in I.U.) of different plaque constituents i.e. calcification, fibrous, necrotic core, and lipid core in four coronary plaques (A, B, C and D) shown in Figure 4. Combined multi-contrast ex vivo PD weighted, T1 weighted and T2 weighted MR images were used for area measurement of each constituent and its % MR signal intensity (in arbitrary units) on any of the image set showing it highest MRI visible.**

| Constituent | Area of constituents($mm^2$) | | | | % MR Signal Intensity(I.U.) | | | |
|---|---|---|---|---|---|---|---|---|
| | Plaque A | Plaque B | Plaque C | Plaque D | Plaque A | Plaque B | Plaque C | Plaque D |
| Total Plaque | 1.1 | 2.41 | 2.34 | 2.98 | 100 | 100 | 100 | 100 |
| Calcification | 0.24 | 1.09 | 0.49 | -- | 21.8 | 4.5 | 21.3 | 24.5 |
| Fibrous Tissue | 0.14 | -- | -- | 0.16 | 10.4 | -- | -- | 5.1 |
| Cholesterol | -- | 0.65 | -- | -- | -- | 2.7 | -- | -- |
| Matrix | -- | 0.24 | -- | -- | -- | 9.3 | -- | -- |
| Lipid Core | -- | -- | 1.17 | 0.42 | -- | -- | 5.0 | 1.4 |
| Necrotic Core | 0.54 | 0.50 | 0.38 | 1.00 | 4.9 | 2.1 | 16.2 | 3.3 |
| Unclassified Core | 0.23 | 0.55 | 0.27 | 0.19 | -- | -- | -- | -- |

absolute scale for computing outer radius-wall thickness ratio and vessel area from MR images of the coronary arteries and the matched histopathology sections [6].

The height of the largest plaque in coronary artery of each rabbit was measured. The total extent of atherosclerotic coronary involvement was assessed by the coronary atherosclerosis index [7]. The frequency of plaques, plaque height in aorta and coronary artery were obtained by atheroma scoring for each animal and the product was divided by the body weight of the animal [8]. Disrupted plaque sections stained with Hematoxylin and Eosine. Disrupted plaques had overlying thrombus. Non-disrupted plaques did not have overlying thrombus [9].

**Table 4: Comparison of histomorphometric measurements and ex vivo MRI visible coronary artery thrombus features of coronary artery serial segments. % aorta wall thickness (mm), atheroma size ($mm^2$) and total plaque volume($mm^3$) were measured by superimposed delineation of area on both histology and MRI images.**

| Rabbit slice[a] Rabbit segment[b] % difference | Total artery radius and area | | | | % Aorta wall thickness (mm) | Atheroma area ($mm^2$) | % Stenosis | Plaque Volume ($mm^3$) |
|---|---|---|---|---|---|---|---|---|
| | Outer Radius (mm)/ Area ($mm^2$) | | Lumen Radius (mm)/ Area ($mm^2$ | | | | | |
| 115_1 | 1.70 | 9.08 | 1.47 | 6.79 | 25.22 | -- | -- | 1.95 |
| 115_seg0.5 | 1.69 | 8.97 | 1.46 | 6.69 | 25.93 | 0.68 | 10.0 | 1.92 |
| **% difference** | **1.0** | **1.2.** | **0.68** | **10.0** | **2.73** | | | **1.53** |
| 120_4 | 1.69 | 8.97 | 1.42 | 6.33 | 29.43 | 0.82 | 12.9 | 2.10 |
| 120_seg1.5 | 1.68 | 8.87 | 1.41 | 6.24 | 29.65 | 0.78 | 12.5 | 1.99 |
| **% difference** | **1.00** | **1.11** | **0.70** | **1.42** | **0.74** | **4.87** | **3.10** | **5.24** |
| 123_3 | 1.68 | 8.87 | 1.42 | 6.33 | 28.63 | 0.92 | 14.50 | 2.50 |
| 123_seg1.5 | 1.67 | 8.76 | 1.39 | 6.07 | 30.70 | 0.86 | 14.16 | 2.60 |
| **% difference** | **0.59** | **1.24** | **2.11** | **4.10** | **7.23** | **6.52** | **2.34** | **3.84** |
| 123_6 | 1.71 | 9.18 | 1.33 | 5.55 | 39.55 | 1.14 | 20.54 | 2.80 |
| 123_seg1.0 | 1.70 | 9.08 | 1.30 | 5.30 | 41.62 | 1.12 | 21.13 | 2.35 |
| **% difference** | **0.58** | **1.09** | **2.25** | **4.50** | **4.97** | **1.75** | **2.79** | **16.0** |
| 133_2 | 1.68 | 8.87 | 1.35 | 5.73 | 35.40 | 0.84 | 14.65 | 2.20 |
| 133_seg2.0 | 1.66 | 8.65 | 1.30 | 5.30 | 38.73 | 0.82 | 15.47 | 2.15 |
| **% difference** | **1.19** | **2.48** | **3.70** | **7.50** | **9.32** | **2.38** | **5.30** | **2.27** |
| 133_4 | 1.67 | 8.76 | 1.42 | 6.33 | 27.74 | 0.86 | 13.58 | 1.80 |
| 133_seg2.5 | 1.66 | 8.65 | 1.34 | 5.64 | 34.80 | 0.74 | 13.12 | 1.65 |
| **% difference** | **0.59** | **1.25** | **5.63** | **10.9** | **20.2** | **13.9** | **3.38** | **8.33** |
| 145_6 | 1.78 | 9.18 | 1.50 | 7.07 | 22.98 | | -- | -- |
| 145_seg2 | 1.67 | 8.76 | 1.45 | 7.00 | 20.10 | 0. 44 | 6.2 | 0.40 |
| **% difference** | **6.17** | **4.57** | **3.33** | **1.0** | **12.53** | | | |
| 145_8 | 1.80 | 10.18 | 1.30 | 5.30 | 47.93 | 1.18 | 22.26 | 2.60 |
| 145_seg4 | 1.77 | 9.84 | 1.28 | 5.14 | 47.76 | 1.06 | 20.62 | 2.35 |
| **% difference** | **1.66** | **3.33** | **1.54** | **3.02** | **0.36** | **10.1** | **7.36** | **9.61** |
| 195_4 | 1.72 | 9.29 | 1.40 | 6.15 | 33.70 | 0.76 | 12.35 | 2.55 |
| 195_seg2.5 | 1.70 | 9.08 | 1.37 | 5.89 | 35.10 | 0.77 | 13.07 | 2.80 |
| **% difference** | **1.11** | **2.26** | **2.14** | **4.22** | **3.98** | **1.31** | **5.50** | **8.92** |
| 195_10 | 1.77 | 9.84 | 1.39 | 6.07 | 38.31 | 0.84 | 13.83 | 2.75 |
| 195_seg | 1.67 | 8.76 | 1.37 | 5.90 | 32.64 | 0.80 | 13.56 | 2.68 |
| **% difference** | **5.65** | **10.9** | **1.43** | **2.80** | **14.80** | **4.76** | **1.95** | **2.54** |
| 195_12 | 1.70 | 9.08 | 1.36 | 5.81 | 36.0 | 0.46 | 11.1 | 1.80 |
| 195_seg | 1.68 | 8.87 | 1.32 | 5.47 | 38.3 | 0.42 | 11.3 | 2.00 |
| **% difference** | **1.10** | **2.31** | **2.94** | **5.85** | **6.00** | **8.69** | **1.76** | **11.1** |
| 195_14 | 1.72 | 9.29 | 1.32 | 5.47 | 41.11 | 0.58 | 10.60 | 1.80 |
| 195_seg | 1.71 | 9.18 | 1.33 | 5.55 | 39.54 | 0.60 | 10.81 | 1.55 |
| **% difference** | **0.58** | **1.18** | **0.75** | **1.44** | **3.82** | **3.33** | **1.94** | **3.12** |
| 198_3 | 1.71 | 9.18 | 1.36 | 5.47 | 40.4 | 1.14 | 28.84 | 2.20 |
| 198_seg1.5 | 1.67 | 8.76 | 1.30 | 5.30 | 39.5 | 1.10 | 20.75 | 2.10 |
| **% difference** | **2.33** | **4.57** | **4.41** | **3.10** | **2.22** | **3.50** | **28.0** | **4.54** |
| 198_5 | 1.68 | 8.87 | 1.39 | 6.06 | 31.68 | 1.15 | 18.97 | 1.20 |
| 198_seg2.0 | 1.60 | 8.04 | 1.34 | 5.64 | 29.85 | 1.12 | 19.86 | 1.55 |
| **% difference** | **16.6** | **9.35** | **3.59** | **6.93** | **5.77** | **2.60** | **4.48** | **4.16** |

[a]Rabbit number and magnetic resonance microimage slice number(1 mm thick). [b]Rabbit number and coronary tissue segment containing corresponding MRM slice(5 mm thick).

### *Atherosclerotic plaque burden and thrombus*

Magnetic resonance images were manually traced for outer wall and lumen area measurement. The area measurements determined the percentage aortic wall thickness [$\simeq$ × 100%] and the percent stenosis of the lumen area [area of thrombus / (area of lumen) × 100%]. These calculations were performed on the coronary artery MR images showing thrombus and the luminal surface of the aortic

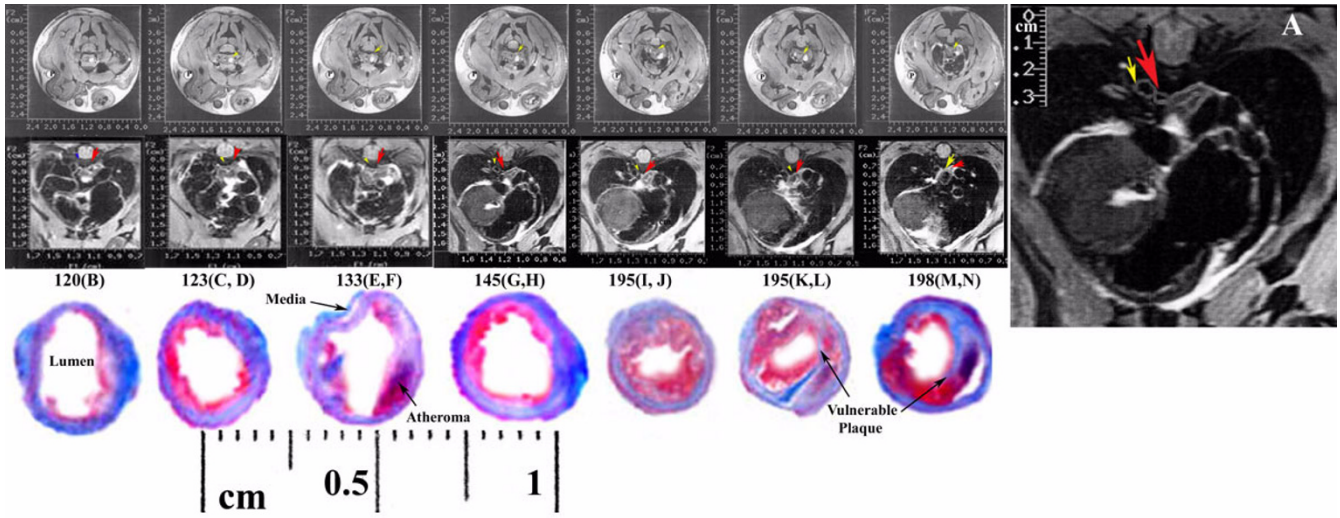


**Figure 1**
Top row: Contiguous in vivo gradient echo MR images are shown with different levels of coronary artery proximal to distal side (left to right) showing three coronary arteries (shown as arrows) with phantom tube (shown as P). Middle row: Note the arterial wall thickness increase (red arrow) and plaque atheroma (yellow arrow) developed around coronary wall at different levels. The insert A represents zoomed view of serial in vivo image in center. Bottom row: Co-registered histology sections of MRI matched coronary artery showing wall thickness and plaque at various levels. Outer adventitia and media layers are shown (blue-purple) and high-risk atheroma and plaques are shown as red obstructing lumen.

wall [8]. The corresponding histological sections of the aorta stained with trichrome-mason were put on a projecting microscope (Microprojector model 1202, Carl Zeiss, Inc) and were projected onto a digitizing tablet. The luminal, medial, and outer wall areas were manually traced and quantified by using NIH Image 1.63 Analysis Software program (Scion Image). The percent aortic wall thickness and percent stenosis were determined histologically by the manner as described above for MRI. By using the distance from the right coronary artery as the point of reference, comparative analyses were performed with the MRI scans at the same level [9].

### *MR microimaging and histology image postprocessing*

MR microimages were adjusted for high contrast using 'Sun VNMR' software. These images were displayed on a Sun Sparc 5 workstation. Similarly, histology slides were photographed with Olympus D-320 L Digital Vision camera and the colored digital images were projected with a microimage Video system and Ikegami 370 M control unit onto a SONY Trinitron super fine pitch screen for area computation using Optimas 6.5 software. Data for histology and MR images were compared and statistically analyzed using PRISM 3 software [10].

### *Statistical analysis*

For optimization, MRI data were reported as % signal intensities. MRI and histology data were reported as mean ± 1 SD. Comparisons were done by percent difference and correlations were made by paired t test, least-squares linear regression. Differences were significant if the two-foiled value was < 0.05 [10].

## Results

### *MR imaging and coronary artery specimens*

In vivo MR images and corresponding ex vivo MR images with serial histology sections are shown in Figure 1. Gradient echo images showed right coronary artery as bright (panels on top row). Spin echo images enlarged view showed main three coronary arteries as shown with arrows in Figure 1(panels on middle rows). Coronary artery endarterectomy specimens were removed from these three coronary arteries viz. RCA (top), LAD (middle) and LCx (bottom) as shown in Figure 2.

Selection of MRI image scan parameters generated three T1-weighted, T2-weighted and proton density-weighted images that further enhanced the contrast as shown in Figure 3 (arrows on three panels in top row). In Figure 3, T1 weighted (left panel), proton density-weighted (middle panel) and T2-weighted (right panel) showed different signal intensities suggestive of distinct plaque

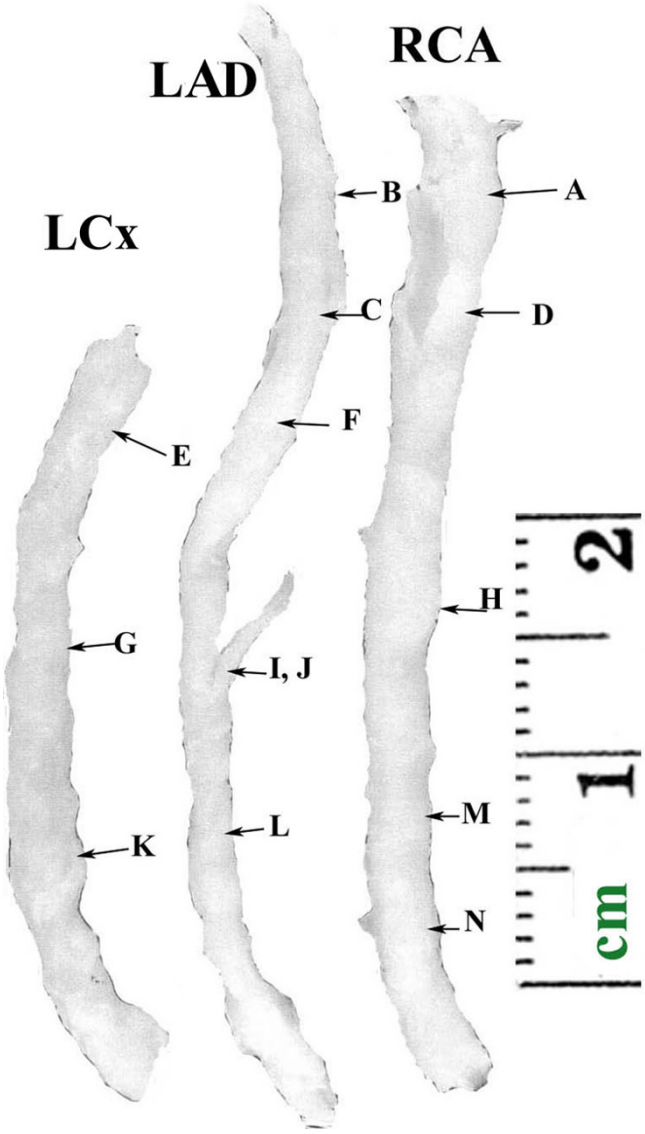


**Figure 2**
Three endarterectomy coronary artery specimens are shown on left panel. These specimens were excised after in vivo MR imaging shown in Figure 1.

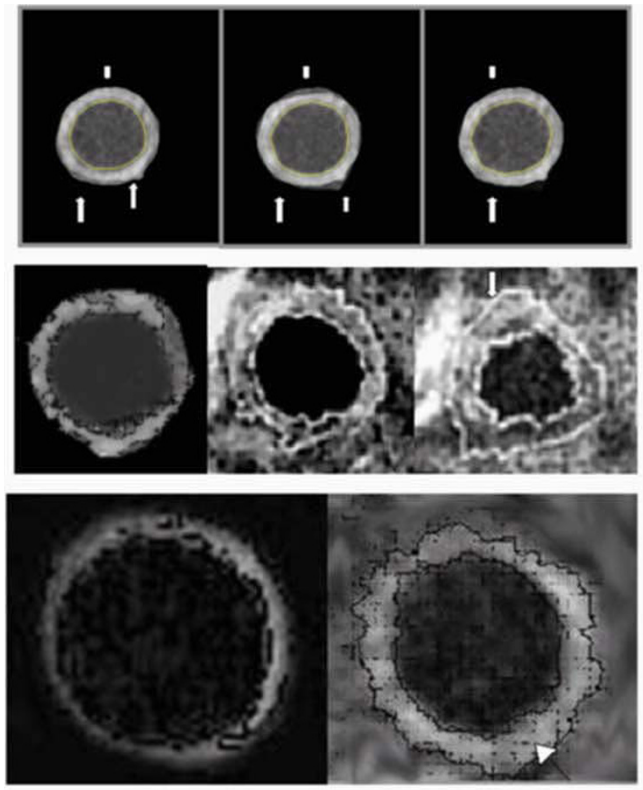

**Figure 3**
Top Row: A coronary plaque is shown on three different ex vivo MRI images: T1 weighted (left panel), proton density weighted (middle panel) and T2 weighted (right panel) showing different signal intensities) suggestive of distinct plaque components i.e. calcification (right arrow on bottom), fibrous, thrombotic core (left arrow on bottom), and lipid core (arrow on top). Note that each plaque component shows specific signal intensity at different T1/T2 and proton density weighting. Middle Row: Delineation of wall thickness and lumen area is shown on ex vivo MRI image (left panel) and corresponding in vivo image (middle panel) and atheroma (arrow in right panel). Bottom Row: A comparison of wall thickness is shown in a normal coronary artery image (left panel) and coronary artery image with thick wall and atheroma (right panel).

components. Each plaque component showed specific signal intensity at different T1/T2 and proton density weighting. Delineation of wall thickness, lumen area on ex vivo MRI images and corresponding in vivo images distinguished atheroma. The Wall thickness measurement in a normal coronary artery distinguished the thrombosis seen as thick wall and atheroma seen as narrow lumen in its cross-sectional magnetic resonance images. The thrombosis and control coronary aorta are shown in Figure 3 (panels at middle and bottom rows). Thick coronary aorta with thrombosis had circular lumen. Similarly, control coronary aorta cross-sections showed circular lumen from another rabbit as shown in Figure 3.

### *Extent and quality of atheroma formation*

The mean score of sudanophilia was greater in atherosclerosis group rabbits. The aortic and coronary artery plaque heights, as revealed by micrometer, were significantly greater in the atherosclerosis group compared with control group with no plaque (see Table 1). Coronary

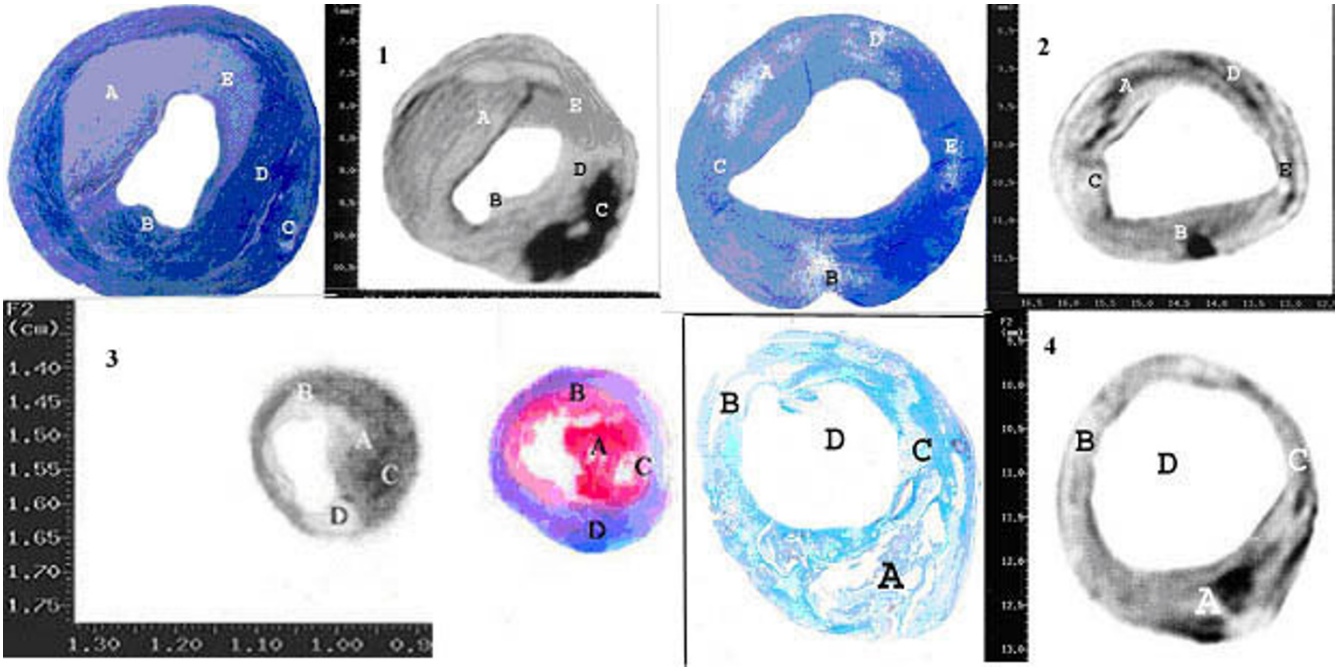


**Figure 4**
The figure represents four coronary plaques ex vivo T2-w MRI images acquired with a 9.4 T MRI scanner for the segmentation of different plaque components at different levels. For comparison, corresponding histology sections are shown with different plaque constituents (A, B, C and D) with dark calcification, gray lipid core and bright fibrous core.

atherosclerosis index, aortic atherosclerosis score, and coronary atherosclerosis score were significantly lower in control group animals. A variable degree of medial thickening was observed in both rabbit groups, as revealed by paraffin sections of aortic and coronary arteries. Fatty streaks, atherosclerotic plaques and fibrous plaques were observed in atherosclerosis group animals. Rabbits showed myocardial muscle degeneration and mural thrombus in coronary arteries. On histology, all rabbits had evidence of atherosclerosis, as indicated by medial thickening.

The quality of atheroma revealed that control group rabbits showed significantly more ulceration, hemorrhage, and thrombosis, indicating complicated lesions in the coronary arteries. Assessment in general by appearance revealed the plaques as atheromatous, fragile, with cracks or fissures and appeared lipid rich.

### *Comparison and analysis of the histomorphometric and ex-vivo MRI features of coronary aortic images*

A contiguous series of representative ex vivo MR microimaging (MRM) slices 1 mm thick with in-plane resolution of 0.1 mm is shown (Figure 4, right panels in 2 rows). These slices enabled the identification of heterogeneous atheroma components appearing as dark, gray and bright areas. In these images, extensive occlusion of coronary artery showed as darker calcification and crystalline cholesterol (Figure 4, left panels). Prominent necrotic core (~0.25 mm diameter), media thickening (0.05 – 0.15 mm), circular lumen diameter (1–2 mm) with massive atheroma accumulations was a main feature. MRM visualized (Figure 4, panels in 2 rows) specific features of atheroma size, % wall thickness, % stenosis and plaque volume. Figure 4 shows atherosclerosis-rabbit coronary artery magnetic resonance images of the aortic cross sections, with each showing a crescent shaped mass/thrombus. The corresponding histological sections confirmed the thrombus within the lumen of the aorta at these levels. A thrombus was also seen in MRI image and was confirmed by histological analyses of the corresponding sections.

Another example of registered MRM image slice and histologic image showed a intact lumen, stenosed necrotic core occluded with thrombi (Figure 4, right panel at bottom). Histopathology features represented several distinct plaque type III and IV components possibly fibrin intermixed with cholesterol and necrotic core, fibrous cap intact towards lumen feature and collagen or

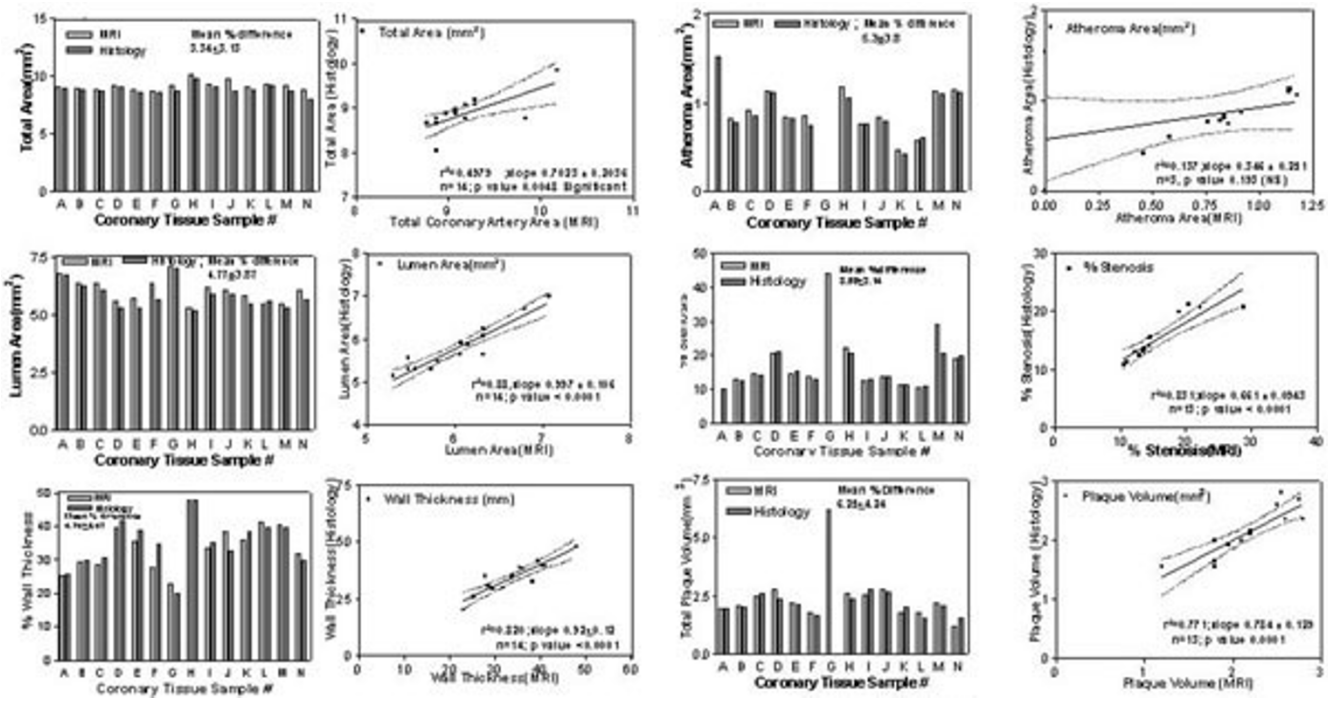


**Figure 5**
Comparison as histogram bars (panels on left) and regression analysis (panels on right) showing correlations of total area, lumen area, wall thickness, atheroma area, artery luminal stenosis, plaque volume by histology method with respective MRI. Plaque feature areas for distinct histological features are shown comparable with MRI image measurement.

proteoglycan shown in Figure 4. Calcification was distinguished as black or no signal (see Figure 4, feature C on top left and feature A at bottom right panels) that showed space in histology sections.

Quantitative comparison of total artery radius and area, thickness of the aortic wall, lumen area from MRM and histological samples was made as shown in table 4 as histogram bars (o n left) and corresponding correlation (on right) (figure 5). The MRM values and the histological values showed correlation shown in Figure 5. The linear regression was calculated for total wall areas ($r^2 = 0.498$; p value 0.0048); lumen areas ($r^2 = 0.881$; $p < 0.0001$); percent wall thickness ($r^2 = 0.820$; $p < 0.0001$); coronary luminal % stenosis ($r^2 = 0.831$; $p < 0.0001$). The percent luminal stenosis was (mean ± SD) determined by comparing atherosclerotic aorta MRM with their respective control MRM images. The location of thrombus was defined as the most distal point of the thrombus from the artery. Thrombus area showed insignificant correlation ($r^2 = 0.137$; $p < 0.193$) between histology and MRI. Similarly, there was a correlation ($r^2 = 0.771$; $p < 0.0001$) between plaque volumes by MRM and histology. The total area measurement showed correlation by T2-w MRM ($r^2 = 0.646$; p 0.008) over MRI ($r^2 = 0.488$; $p < 0.006$) with histology.

### *Contrast enhancement and resolution*

Two approaches were used to improve resolution viz. 3D plots for lipid rich atheroma / fibrous tissue at 9.4 T and parametric imaging. Figure 6 and Table 5 show 3D plots revealing that a high contrast of 0.25 can be achieved using a very short TE (~4 ms) and short TR (~500 ms) and lower contrast of ~0.12 may be obtained at more accessible parameters TR = 2–3 sec; TE = 50–100 ms. In second 'discriminant analysis' approach, T1-, T2- and proton density-weighted image intensities categorized tissue components with color display (right panel of Figure 6).

With a multicontrast protocol using T1-weighted, T2-weighted images and proton density-weighted images showed coronary tissue features as shown in Figure 6. Image intensities of different locations on these images indicated that some areas were better MRI-visible on T1-weighted, T2-weighted or proton density weighted images. So, gray levels for any location on these images may characterize coronary artery better by combining the

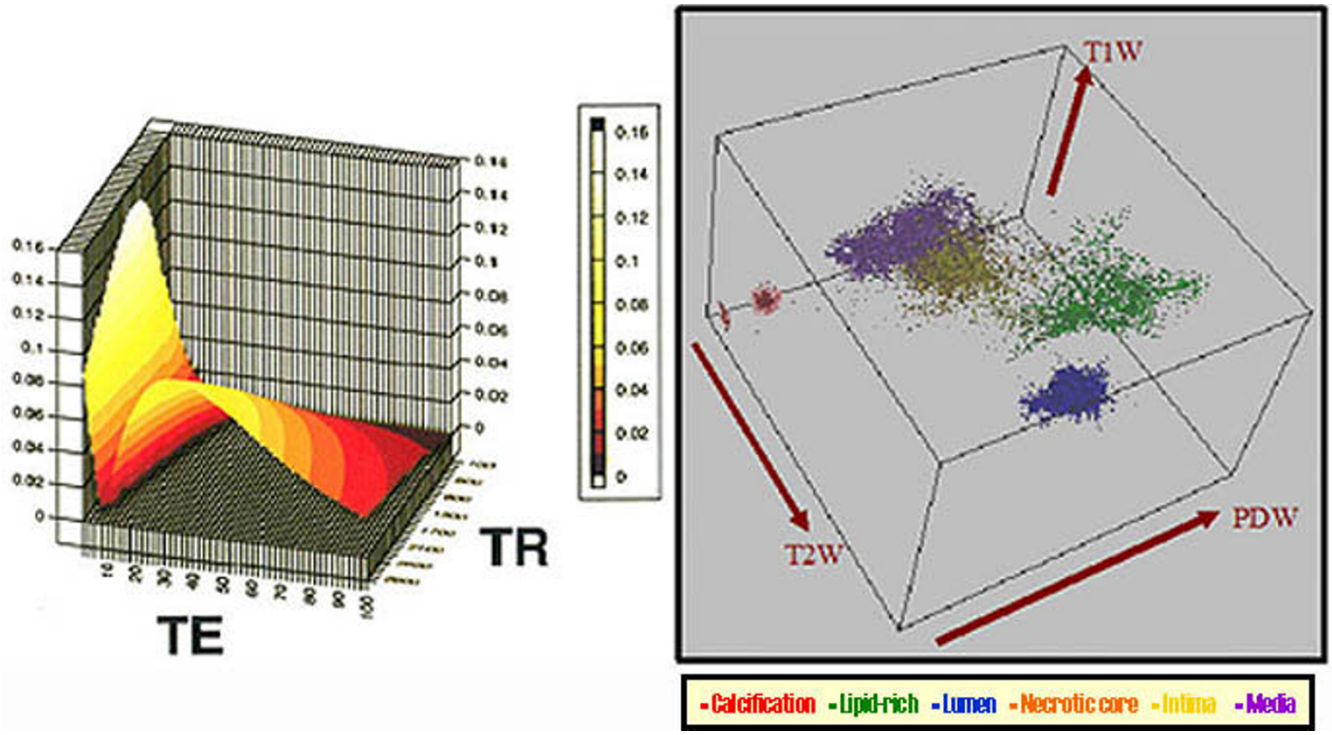


**Figure 6**
Dependence of image contrast for lipid rich atheroma and fibrous tissue is shown as 3D plot (left panel). Note the image contrast between atheroma and fibrous tissue as a function of unique combination of scan optimized parameters-TE and TR, at 9.4 T. Multicontrast method is represented to demonstrate different feature space intensity 3D distributions of plaque components using combined T1-w, T2-w and proton density weighting.

**Table 5: Optimization of MRI spin echo parameters TE and TR for T2 parametric contrast enhancement between atheroma and fibrous tissue at 9.4 T (see Figure 6). Different combinations of TE and TR generate T1-, proton density- and T2- weighting and their relative appearance on gray scale.**

| TR (ms) | TE (ms) | MRI Signal Intensity on gray scale |
|---|---|---|
| 2000 | 10–30 | dark; heavy T1 wt |
| 2000 | 20–40, 50–80 | gray; medium T1 wt |
| 1000 | 2–10 | bright; T2 wt |
| 1000 | 30–70 | dark; heavy T1 wt |
| 800 | 10–20 | gray; medium T1 wt |
| 200 | 20–70 | dark; heavy T1 wt |

contrast information of that location on these three images.

*Sensitivity and specificity*

Table 6 shows the results of the relative signal intensity (CV %), sensitivity and specificity of the MRI criteria for evaluation of T2 weighted parametric images (panels at bottom of Figure 7). Thrombus component showed lowest sensitivity. However, thrombi next to calcification were poorly visible on MRI because of dark areas of calcified tissue. Other regions of collagen, lipid, and fibrous features were better MRI visible and distinct by histology examination.

**Table 6: Sensitivity and specificity of ex vivo coronary artery MRI at spin echo (TE = 50 ms) and T2 image (panel on right). Different artery atheroma features are represented with reference to coronary artery image for distinct tissue components and corresponding T2 parametric image (A) of coronary endarterectomy specimen and right postsegmented image (B) showing different signal intensities (CV %) and their relative appearance on gray scale with varying T2 ranges for different atheroma components.**

| Atheroma features | Signal intensity (CV %) | Sensitivity (%) | Specificity (%) | T2-wt (TE = 50 ms) |
|---|---|---|---|---|
| Calcium | Dark | 100 | 100 | Dark |
| Collagen | 14.5(18 %) | 95 | 85 | Bright |
| Lipids | 23.0(7.5 %) | 90 | 75 | Dark |
| Lipid core | 27.5(7.5%) | 100 | 100 | Gray |
| Fibrous | 35.5 (7 %) | 85 | 90 | Bright |
| Elastin | 40.7 (13.5 %) | 70 | 80 | Gray |

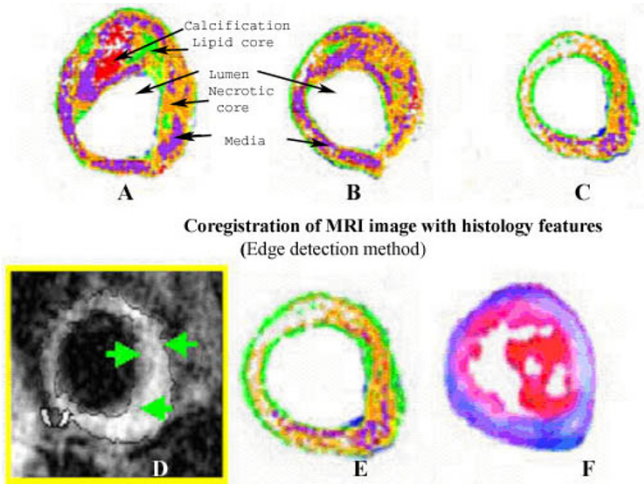


**Figure 7**
Different artery atheroma features are represented on coronary artery postsegmented feature map images for distinct plaque components and media layer (first and second panels on top). The combinations of different signal intensities (panels A-F) predict the distinct color-coded plaque feature(s) by using robust VTK program. At bottom, a proton density in vivo MRI image (left panel) shows dark areas of fibrous layer (arrow), lipid rich regions (gray areas open arrow). T2 parametric in vivo image (left panel) is shown with corresponding postsegmented image (middle panel) with corresponding coronary artery histology section showing different areas corresponding with varying T2 ranges for different atheroma components shown in Table 6. On histology sections, matrix appears bluish, calcification show gaps, atheroma as red and continuous fibrous layer.

Table 7 summarizes the relative ex vivo MRI visibility of different excised tissues using T1-, T2- and proton density weighted (multicontrast) approach with their relaxation times.

## Discussion

An atherosclerotic rabbit model of coronary plaque rupture was used. *In vivo* MRI and *ex vivo* MRM identify and quantify atheroma contents and plaque volume in rabbits after treatment of vegetable ghee. MRI data and histology data showed correlation between measurements of aortic wall thickness, aortic luminal area, % stenosis and thrombus size. Present study adds new information of coronary thrombus MR characteristics and relaxation times, optimization of MRI scan parameters and comparison of MRI-histopathological quantitation for coronary artery morphometric features. The changes seen in control and atherosclerosis MRI support the development of thrombus in experimental rabbits, occurs after treatment of vegetable ghee. Coronary thrombosis was observed during lipid peroxidation. Since the control group animals received no antioxidants as a result showed more atherosclerosis.

Wall shear stress, turbulence, atheroma formation affect the MR visibility and make routine coronary magnetic resonance angiography inconclusive for composition of the wall, thrombus from underlying atheroma and plaque disruption [11]. As a result, there has been considerable interest in the use of MRI and MRM for the noninvasive assessment of coronary atherosclerosis by using gradient echo (bright blood pool) and spin-echo (dark blood pool) imaging. MRM can evaluate the composition of vulnerable plaque to disruption in order to assess the cardiovascular risk [12-14]. The present study evaluates these observations. Due to paucity of sufficient information on *in vivo* MR image coronary plaque characterization, *ex vivo* MR image data validation was needed for it. The present study demonstrates the power of in vivo MR imaging accuracy in determination of normal and thrombosed arteries. It further highlights the coronary wall and vulnerable plaque characterization of its components using 1 mm MR slice registration with 4-micron histology section. Thrombi, lumen and wall thickness were

**Table 7: The table represents different plaque constituents and their MRI visible protons in active chemical groups. These different constituents exhibit specific MRI signal intensity determined by their specific relaxation times T1 and T2 at specific 9.4 T magnetic field.**

| Plaque components | Chemical structure | T1(ms) | T2(ms) | MRI Visibility* | | |
|---|---|---|---|---|---|---|
| | | $S = N(1 - e^{-T1/TR})$ | $S = N(1 - e^{-TE/TR})$ | T1-w | T2-w | PD-w |
| Lipid | $-CH_2-CH_2-$ | 1643.3 ± 25.6 | 52.9 ± 2.5 | + | - | +/- |
| Cholesterol | $-CH_3$ | 643.5 ± 34.5 | 14.3 ± 0.9 | + | +/- | +/- |
| Calcium | Bound form | 56.5 ± 10 | 2.2 ± 0.4 | -- | -- | -- |
| Collagen | $-CH_2$ (-Gly-Hyp-Pro-) | 1750.4 ± 25.4 | 54.1 ± 0.8 | + | +/- | + |
| Elastin | $-CH_2-\underline{N}H_2$ | 1640.6 ± 16.2 | 62.2 ± 1.1 | +/- | +/- | + |
| Atheroma | Paramagnetic Heme | 1204.2 ± 14.4 | 16.0 ± 1.2 | + | - | - |

* The relative gray scale MR signal intensity is shown as +(bright hyperintense), +/-(gray isointense), -(dark hypointense) on T1-weighted, T2-weighted and proton density(PD) weighted images.

measurable by using in vivo MRI in an animal model more accurately than previous reports [12-14]. The MR visibility was based upon the assumption that plaque components viz. lipid, collagen, calcium, cholesterol, hemorrhage, fibrin etc. show different T1, proton density and T2 signal intensities depending upon their chemical structure and relaxation values as shown in Table 7.

Multi-contrast approach identified dense fibrocellular, lipid rich and calcified regions of atherosclerotic plaque. Plaque atheroma appeared as less dense as corroborating with earlier report [16]. Our data using spin-echo short TE, T2 weighted MRM confirm the sensitivity of MRI in the evaluation of stenosis and aortic wall thickness reported earlier [9]. Our MRI results did not demonstrate thrombi and measurable degree of stenosis on control coronary artery images. It confirms the previous report [1] on development of a thrombus after treatment of vegetable ghee leading to vulnerable plaques or stenotic plaques. However, the role of excessive trans-fatty acids in thrombus development due to vegetable ghee rich diets is poorly known [2].

At 9.4 T, in-plane resolution of 512 × 256 micrometers distinguished the plaque components in contiguous MRM slices e.g. lipid-rich protons, fibrous tissue appearing as brighter, calcium deposits appearing as darker, and measured the size of coronary wall thickness, lumen, and plaque area. However, histological specimen shrinkage caused overestimation of wall area, lumen area and stenosis if compared with true measurements.

In coronary magnetic resonance imaging, contrast enhancement was reported by using T1 and T2 different preparation phases and fat-suppressed gradient echo images. Proton density weighted and T2 weighted MRM images at different levels of brightness provided high SNR and distinct plaque atheroma components [8]. Most investigators reported spin-echo sequences for atherosclerosis plaque showing darker lipid rich core and lighter fibrocellular tissue by T2 weighted sequences. However, T2-weighted hypointensity and T1-weighted hyperintensity of hemorrhage and fibrous tissue made distinction of hemorrhage, fibrous tissue and atheroma [15,16]. In present report, atheroma and fibrous content in coronary plaque images generated optimized contrast at different TE and TR values. Present study corroborates with earlier observations of T2 weighted contrast using broad range of TR and TE values [5].

Parametric imaging of segmentation and quantification of plaque components based on their TE and TR values could be accomplished with high degree of sensitivity and specificity. These TE/TR optimized values appear to provide information of noninvasive in vivo application of MRI criteria. T2-weighted signal intensities micro-dissected the necrotic core at different sets of TE values. However, T2-w images showed plaque thrombus and fibrous components as darker. T1 weighted images provided less information than T2 weighted images or proton density weighted images. So, it needs appropriate TE and TR optimized choice for T2-weighted *in vivo* MR microimaging application.

### *Limitations of the study*

The comparative analysis of MRI with the histological sections showed measurable differences. The fresh frozen tissue histology technique suffers from shrinkage in thrombus size. This results in tissue shrinkage and shape deformation, which may lead to underestimation of the true lumen size. Furthermore, the ex vivo rabbit aorta is also subject to shrinkage lengthwise after dissection. The accuracy of thrombus location by histology is further compromised by the estimation of the distance of the thrombus from the ends of the 1-mm slices. It needs correction factor to minimize the impact of shrinkage. Our previous study suggested that the lipid content in vegetable ghee lipids as important factor in determining plaque

vulnerability as lipid disorder in rabbit experimental model [2]. However, differentiation of lipid from fibrous or small thrombotic components of the coronary artery with the use of MRI is difficult because of the large pixel size compared with smaller coronary plaque thickness in this animal model. In the vicinity of coronary stenosis region, the magnetic resonance signal void is minimum due to turbulence and results with loss in stenosis details. Availability of intravascular MRI coils may enhance the chance of better plaque thrombus characterization. Unfortunately, such technical advanced modifications are both invasive and expansive, therefore, less promising. Other possible improvements of MRI techniques such as diffusion weighting, high gradient strength, and a combination of T2-weighted imaging with 1-H spectroscopy have been reported [17,18]. These developments and such advances may help to determine plaque vulnerability and its type.

## Conclusion

In a rabbit model of atherosclerosis and plaque rupture, we demonstrate the multicontrast approach of in vivo and ex vivo MRI to determine the plaque burden, size of a thrombus and its accuracy by histology in the rabbit aorta after vegetable ghee treatment.

## Acknowledgements

Authors acknowledge the support for this imaging and histology data analysis at Heart Research Lab with R.B. Singh. First author acknowledges Figures 1, 2 and 6 as part of MRI training with Professor J.D. Morrisett, Texas Medical Center, Houston, Texas and Drs Paul J. Canon and Dan Burkoff, Cardiology Division, Department of Medicine, Columbia University, New York, New York 10033 for the access to their lab and computer analysis facility.

## References

1. Singh RB, Shinde SN, Chopra RK, Niaz MA, Thakur AS, Onouchi Z: **Effect of coenzyme Q10 on experimental atherosclerosis and chemical composition and quality of atheroma in rabbits.** *Atherosclerosis* 2000, **148(2):**275-82.
2. Pella D, Dubnov G, Singh RB, Sharma R, Berry EM, Manor O: **Effects of an Indo-Mediterranean diet on the omega-6/omega-3 ratio in patients at high risk of coronary artery disease: the Indian paradox.** *World Rev Nutr Diet* 2003, **92:**74-80.
3. Naghavi M, Libby P, Falk E, *et al.*: **From vulnerable plaque to vulnerable patient: a call for new definitions and risk assessment strategies: Parts I.** *Circulation* 2003, **108(14):**1764-72. Ibid: **Part II** *Circulation*. 2003; **108(15)**: 1772–78.
4. Worthley SG, Helft G, Fuster V, Fuster V, Fayad ZA, Rodriguez OJ, Zaman AG, Fallon JT, Badimon JJ: **Noninvasive in vivo magnetic resonance imaging of experimental coronary artery lesions in a porcine model.** *Circulation* 2000, **101:**2956-2961.
5. Sharma R: **Carotid MRI plaque characterization in Atherosclerosis:.** *Magnetic Resonance in Medical Science* 2002, **1(4):**217-233.
6. Chakravorti RN, Mohan AP, Komal HS: **Atherosclerosis in Macca mulatto: histopathological, morphometric and histochemical studies in aorta and coronary arteries of spontaneous and induced atherosclerosis.** *Experimental Molecular Pathology* 1976, **25:**390-401.
7. Bansal N, Majumdar S, Chakravorti RN: **Frequency and size of atherosclerosis plaques in vasectomized diabetic monkeys.** *International Journal of Fertility* 1986, **31:**298-304.
8. Johnstone MT, Botnar RM, Perez AS, Stewart R, Quist WC, Hamilton JA, Manning WJ: **In vivo Magentic Resonance Imaging of experimental thrombosis in rabbit model.** *Arterioscler Thromb Vasc Biol* 2001, **21:**1556-1560.
9. Morrisett J, Vick W, Sharma R, Lawrie G, Reardon M, Ezell E, Schwartz J, Hunter G, Gorenstein D: **Discrimination of components in atherosclerotic plaques from human carotid endarterectomy specimens by MRI in vivo.** *Magnetic Resonance Imaging* 2003, **21(5):**468-474.
10. Traub O, Berk BC: **Laminar shear stress: mechanisms by which endothelial cells transducer an atheroprotective force.** *Arterioscler Thromb Vasc Biol* 1998, **18:**677-685.
11. McConnell MV, Aikawa M, Maier SE, Ganz P, Libby P, Lee RT: **MRI of rabbit atherosclerosis in response to dietary cholesterol lowering.** *Arterioscler Thromb Vasc Biol* 1999, **19:**1956-1959.
12. Worthley SG, Helft G, Fuster V, Zaman AG, Fayad ZA, Fallon JT, Badimon JJ: **Serial in vivo MRI documents arterial remodeling experimental atherosclerosis.** *Circulation* 2000, **101:**586-589.
13. Skinner MP, Yuan C, Mitsumori L, Hayes CE, Raines EW, Nelson JA, Ross R: **Serial magnetic resonance imaging of experimental atherosclerosis detects lesion fine structure, progression and complications in vivo.** *Nat Med* 1995, **1:**69-73.
14. Worthley SG, Helft G, Fuster V, Fayad ZA, Shinnar M, Minkoff LA, Schechter C, Fallon JT, Badimon JJ: **A novel nonobstructive intravascular MRI coil: in vivo imaging of experimental atherosclerosis.** *Arterioscler Thromb Vasc Biol* 2003, **23(2):**346-50.
15. Pohost GM, Fuisz AR: **From the microscope to the clinic: MR assessment of atherosclerotic plaque.** *Circulation* 1998, **98:**1477-1478.
16. Worthley SG, Helft G, Fuster V, Fayad ZA, Fallon JT, Osende JI, Roque M, Shinnar M, Zaman AG, Rodriquez OJ, Verhallen P, Badimon JJ: **High resolution ex vivo magnetic resonance imaging of in situ coronary and aortic atherosclerosis plaque in a porcine model.** *Atherosclerosis* 2000, **150:**321-329.
17. Toussaint JF, Southern JF, Fuster V, Kantor HL: **Water diffusion properties of human atherosclerosis and thrombosis measured by pulse field gradient nuclear magnetic resonance.** *Arterioscler Thromb Vasc Biol* 1997, **17:**542-546.
18. Choudhury RP, Fuster V, Badimon JJ, Fisher EA, Fayad ZA: **MRI Characterization of atherosclerosis plaque: Emerging applications and molecular imaging.** *Arterioscler Thromb Vasc Biol* 2002, **22:**1065-1074.